



OPEN

SUBJECT AREAS:

ELECTRONIC PROPERTIES
AND MATERIALSSURFACES, INTERFACES AND
THIN FILMS

TWO-DIMENSIONAL MATERIALS

SOLAR CELLS

Received
24 January 2013Accepted
28 May 2013Published
12 June 2013

Correspondence and
requests for materials
should be addressed to
C.G.Z. (cgzeng@ustc.
edu.cn)

* These authors
contributed equally to
this work.

Giant photovoltaic effects driven by residual polar field within unit-cell-scale LaAlO_3 films on SrTiO_3

Haixing Liang^{1*}, Long Cheng^{1*}, Xiaofang Zhai¹, Nan Pan¹, Hongli Guo¹, Jin Zhao^{1,2}, Hui Zhang¹, Lin Li¹, Xiaoqiang Zhang¹, Xiaoping Wang¹, Changgan Zeng^{1,2}, Zhenyu Zhang² & J. G. Hou^{1,2}

¹Hefei National Laboratory for Physical Sciences at the Microscale and Department of Physics, University of Science and Technology of China, Hefei, Anhui 230026, China, ²ICQD/HFNL, University of Science and Technology of China, Hefei, Anhui, 230026, China.

For polar/nonpolar heterostructures, Maxwell's theory dictates that the electric potential in the polar components will increase divergently with the film thickness. For $\text{LaAlO}_3/\text{SrTiO}_3$, a conceptually intriguing route, termed charge reconstruction, has been proposed to avert such "polar catastrophe". The existence of a polar potential in LaAlO_3 is a prerequisite for the validity of the charge reconstruction picture, yet to date, its direct measurement remains a major challenge. Here we establish unambiguously the existence of the residual polar potential in ultrathin LaAlO_3 films on SrTiO_3 , using a novel photovoltaic device design as an effective probe. The measured lower bound of the residual polar potential is 1.0 V. Such a direct observation of the giant residual polar potential within the unit-cell-scale LaAlO_3 films amounts to a definitive experimental evidence for the charge reconstruction picture, and also points to new technological significance of oxide heterostructures in photovoltaic and sensing devices with atomic-scale control.

In today's materials science, much research effort is devoted to exploring intriguing emergent properties and potential technological applications at the interface of two dissimilar materials. One particularly active area is related to oxide interfaces, with the growth of polar LaAlO_3 (LAO) overlayers on the nonpolar SrTiO_3 (STO) substrates as a prototypical example^{1–3}. It was discovered that, even though the LAO overlayer and the STO substrate were both insulating, their interface could become conducting with pronounced carrier mobility⁴, suggesting the possible generation of an interfacial quasi-two-dimensional electron gas (q2-DEG)⁵. More recent studies have also shown the existence of ferromagnetism⁶, superconductivity⁷, and even the coexistence of ferromagnetism and superconductivity^{8–11} at the interface.

Ever since the initial report of the LAO/STO interfacial conductivity, there has been active debate^{2,12–19} about the underlying physical origin of the q2-DEG, which in turn is believed to be responsible for many of the intriguing interface phenomena. In the charge reconstruction picture¹³, a net fraction of electron charge is transferred from the LAO surface to the interface above a critical LAO thickness of 4 unit cells (uc), to suppress the divergence of the electric potential associated with the polar field in the LAO overlayer (known as the "polar catastrophe"). Ideally, a complete suppression of the polar field would require a net transfer of 0.5 electron per two-dimensional unit cell¹³, which could occur only for an infinitely thick LAO overlayer^{20,21}. For physically realistic systems with finite overlayer thicknesses, the interface carrier density was consistently much smaller than that expected from the ideal charge transfer picture^{5,20,21}; this incomplete charge reconstruction in turn is expected to be accompanied by the existence of a residual polar potential V_{res} in the overlayer, as shown in the left panel of Fig. 1a^{20–23}. In competition with the intrinsic charge reconstruction picture, extrinsic mechanisms, including oxygen vacancies^{14–17} and interface intermixing^{18,19}, have also been proposed. In these two models, the polar field in the LAO is expected to be minimal^{14,17,18}. Determining the existence of the polar field in the LAO overlayers is thus vitally important in potentially revealing the dominant underlying mechanism for the interfacial q2-DEG. Extensive efforts have been devoted to its measurement under different physical situations, yet to date, highly controversial findings have been reported in these studies using different approaches, and in many cases involving indirect measurements^{18,24–26}. It is therefore highly desirable, and is also of great significance, to firmly establish the existence of the residual polar field using more direct experimental probes.

Here we show the direct observation of such residual polar potentials in the LAO overlayers with a thickness down to a few uc by exploiting the photovoltaic (PV) effect as a more effective and reliable probe, with the

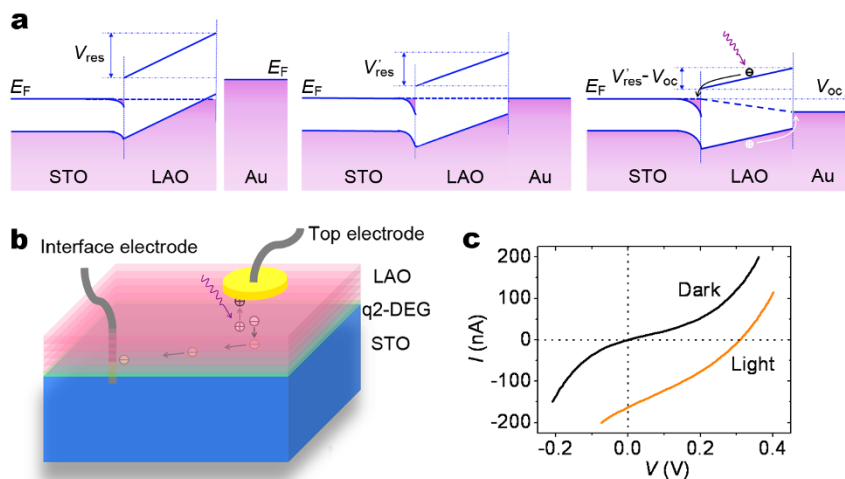


Figure 1 | Band diagram and PV effect. (a) Schematic band diagrams for an LAO/STO heterostructure, an Au/LAO/STO heterostructure, and an Au/LAO/STO heterostructure under UV illumination with photon energy larger than the LAO gap, respectively. The LAO thickness is assumed to be equal to or larger than 4 uc. The dashed lines refer to the Fermi level in the LAO. (b) Schematic of the PV effect across the LAO overlayer in an Au/LAO/STO heterostructure. (c) I - V curves between the surface Au electrode and the LAO/STO interface with an LAO thickness of 5 uc without and with 6.7-eV light illumination.

interfacial q2-DEG serving as a natural electrode. The use of the PV effect is essential in enabling a more definitive characterization of the intrinsic polar potential. Furthermore, the demonstration of PV effects at such an ultimate uc scale is expected to have far-reaching technological impacts as well.

Results

PV effect characteristics. High-quality LAO overlayers were grown on STO(001) substrates with atomic-layer control as described in the Methods. Two types of samples were prepared: one with only *in-situ* postannealing, the other with further postannealing under atmospheric oxygen pressure. Samples with only *in-situ* postannealing were adopted in the PV measurements unless otherwise specified. As depicted in Fig. 1b, the PV effects were detected by current-voltage (I - V) measurements performed at room temperature between a metal electrode on the LAO surface and the q2-DEG at the LAO/STO interface for LAO overlayers of varying thicknesses. The q2-DEG that emerges at the LAO/STO interface serves as a natural and convenient bottom electrode, which allows to directly measure the transport properties across the ultrathin LAO overlayers. In principle, the open-circuit voltage V_{oc} measures the electric potential difference between the LAO/STO interface and the electrode/LAO interface. The presence of a top metal electrode generally leads to additional charge transfer from the metal to the STO near the LAO/STO interface (as will be discussed in more details later), a process that will further reduce the V_{res} in the LAO to V'_{res} as depicted in the middle panel of Fig. 1a. We also note that the positive polar field in the LAO can be completely compensated or even be overturned to be negative by the metal contact having a sufficiently small work function²⁷. In order to ensure such a compensation effect to be as minimal as possible, Au electrodes with a relatively large work function were adopted in the measurements unless otherwise specified.

As observed in Fig. 1c, the rectifying effect in the dark I - V curve is not as distinct as that in typical semiconductor p-n junctions, a phenomenon similar to that occurring in narrow p-n junctions where both sides of the junctions are heavily doped²⁸. In either case, the deviations from the typical rectifying effect stem from electron tunneling through the narrow junctions.

Under the illumination of a 6.7-eV ultraviolet (UV) light, the LAO/STO heterostructure exhibits I - V characteristics with a strong PV effect (Fig. 1c). For a 5-uc-thick LAO overlayer, an open-circuit

voltage of $V_{oc} = 0.31$ V, a short-circuit current of $I_{sc} = 165$ nA, and a filling factor of 31% were obtained for a top electrode of Au with a contact area of 0.0064 cm². The filling factor is relatively low compared with that of semiconductor-based PV devices, likely due to the significantly higher series resistance across the thin LAO layer (of the order of M Ω). The I_{sc} scales linearly with the lateral size of the Au electrode, whereas the V_{oc} remains almost as a constant, as shown in Fig. 2a. This linear scaling is reasonable, because only the excitons excited in the LAO region underneath the Au electrode could contribute to the photocurrent, given the insulating nature of the LAO surface (the latter is to be discussed in more details later). Hereafter, the current density J will be used to represent the photocurrent between the top Au (or other metal) electrode on the LAO surface and the LAO/STO interface.

Exclusion of other possible mechanisms for the observed PV effect. To conclusively identify the observed PV effect to be truly due to the residual polar field, next we analyze several leading factors that may cause undesirable complications in the PV measurement. First, we have checked to ensure that the working principle depicted in Fig. 1a is indeed valid, which demands that the Au electrode is not short-circuited to the q2-DEG, and the LAO surface is insulating. The first condition is evidenced by the observation that the resistance between the surface Au electrode and the q2-DEG is about 5 M Ω , almost two orders of magnitude larger than the resistance of the q2-DEG (about 70 k Ω). The second is evidenced by the resistance between two surface Au electrodes (about 10 M Ω), which has the same order of magnitude as that between one surface Au electrode and the q2-DEG.

Secondly, we rule out the possibility that the charge transfer between the Au electrode and LAO surface could be mainly responsible for the observed PV effect. In doing so, it is necessary to stress that both the directions of the observed photovoltage and photocurrent are consistent with the intrinsic polar field in the LAO. As a rough estimate, the work function of the LAO surface is the sum of the LAO electron affinity (with the bulk value of 2.5 eV²⁹) and the LAO bandgap (with the bulk value of 5.6 eV²⁹, or slightly larger if considering quantum size effects for thinner films). Given the bulk Au work function of 5.3 eV, electron transfer is caused from the Au lead to the STO near the LAO/STO interface, and accordingly the electric potential V'_{res} after Au capping is weaker than the residual polar potential V_{res} before Au capping (see Fig. 1a). This suppression

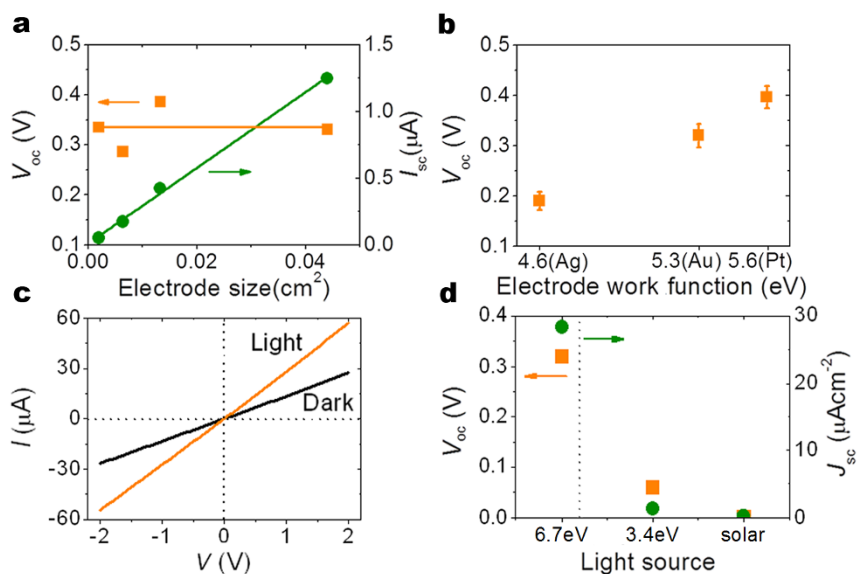


Figure 2 | Detailed I - V characteristics for LAO film thickness of 5 uc. (a) Measured V_{oc} and I_{sc} as functions of the lateral size of the Au electrode. (b) Dependence of V_{oc} on the work function of the surface metal contact. (c) I - V curves of the q2-DEG at the LAO/STO interface in without and with 6.7-eV light illumination. (d) V_{oc} and J_{sc} under UV illumination of 6.7 eV and 3.4 eV with the same incident photon flux ($2.7 \times 10^{16} \text{ cm}^{-2} \text{ s}^{-1}$, which corresponds to 29 mWcm^{-2} for the 6.7-eV light and 15 mWcm^{-2} for the 3.4-eV light). The V_{oc} and J_{sc} measured with a solar simulator (AM 1.5 G filter at 150 mWcm^{-2}) are also shown. The dotted line in (d) refers to the LAO bandgap.

effect in response to a metal contact was also observed in a recent first-principles study²⁷, and also independently confirmed in our present work using physically more realistic models for the Au leads. Details of such calculations are described in the Methods.

The suppression effect described above will be stronger or weaker if a metallic contact with a lower or higher work function is used. Indeed, we found that when a Ag contact with bulk work function of 4.6 eV is used, the V_{oc} is lower; when a Pt contact with bulk work function of 5.6 eV is used, the V_{oc} is higher (see Fig. 2b). It is also noted that surface states on the conventional semiconductors (such as GaAs) generally induce band bending close to the surfaces, which may also lead to PV effect. For such situations, the barrier height (and thus the V_{oc}) is pinned by the surface states, and is therefore almost independent on the work function of the metal electrodes²⁸. In contrast, in the LAO/STO case, the large variation of the V_{oc} in response to the work function change of the metal contact strongly indicates that there is no or little surface states on the LAO surface. Therefore, the observed PV effect can not be attributed to the surface state-induced band bending in the LAO.

Thirdly, we show that the observed PV effect can not be originated from the interface q2-DEG. To rule out this possibility, we used two Al wires directly connected to the interface by ultrasonic welding, as described in the Methods. For this arrangement, both the dark and illuminated I - V curves exhibit linear behavior through the origin (Fig. 2c), indicating good Ohmic contacts at the LAO/STO interface and the corresponding absence of a PV effect from the q2-DEG.

Fourthly, we check the band offset at the LAO/STO interface. In principle, the LAO/STO band offset may also drive a PV effect, if the LAO valence band edge is higher than the STO valence band edge. Controversial findings on the sign of the valence band offset have been reported by X-ray photoelectron spectroscopy measurements^{18,24}. As far as we know, only one experimental study reported that the LAO valence band edge is higher than the STO valence band edge, with a band offset of 0.16 eV¹⁸. The corresponding potential to this value is much smaller than the observed V_{oc} , which can even be larger than 1.0 V as will be shown later. Thus the band offset at the LAO/STO interface can not explain the observed large V_{oc} .

The last and critical aspect to check is that the PV process occurs in the LAO overlayers instead of the STO substrates. This is

accomplished by studying the photon energy dependence of the PV effect. With the same incident photon flux, the V_{oc} and J_{sc} decreased by one order of magnitude from 0.3 V and $28 \mu\text{Acm}^{-2}$ under the 6.7-eV illumination to 0.06 V and $1.4 \mu\text{Acm}^{-2}$ under the 3.4-eV illumination (Fig. 2d, and recall that the threshold energies associated with the bandgaps of LAO and STO are 5.6 eV and 3.2 eV, respectively). The PV characteristic was also measured with a solar simulator in which only a small proportion of the photons possess energy greater than 5.6 eV. In this case, although the light intensity was much stronger (150 mWcm^{-2}), the V_{oc} and J_{sc} were only 0.003 V and $0.33 \mu\text{Acm}^{-2}$, respectively, which are two orders of magnitude smaller than the values under the 6.7-eV illumination. We have also performed measurement across the STO(001) and LAO(001) substrates, with no noticeable PV effect revealed. A previous related study also failed to observe any PV effect on a flat LAO(001) wafer³⁰.

Photoelectric effects have been reported previously based on LAO related materials³⁰⁻³⁴. For example, photoconductivity was observed in the LAO/STO and In-Sn-oxide/LAO/Ag structures, which can be attributed to the photo-generated carriers³¹⁻³³. Such a photoconductivity effect has also been observed here in the q2-DEG at the LAO/STO interface, as shown in Fig. 2c. The central focus of this work is on the PV effect, which exhibits qualitatively different behaviors. Tilted LAO single crystals have been shown to exhibit an ultraviolet PV effect, whose physical origin was attributed to the Seebeck effect³⁰, which should be negligible across the uc-thick LAO overlayer in the present case. We also note that a PV effect was previously revealed in an LAO/Si structure, but with the Si substrate as the active PV region instead of the LAO³⁴. Overall, the previously observed photoelectric effects based on LAO related materials are all distinctly different from the strong PV effect reported here across the uc-thick LAO films on STO substrates.

The experimental LAO/STO systems may contain various disorders, such as oxygen vacancies¹⁴⁻¹⁶ and interface intermixing^{18,19}, both of which would diminish the magnitude of the polar field significantly^{14,17,18}. In order to minimize the negative effects associated with the oxygen vacancies as discussed earlier, the LAO/STO samples with postannealing under atmospheric oxygen pressure were further adopted for the PV measurements. Under 29 mWcm^{-2} illumination, the V_{oc} is 0.58 V for Au electrode and 0.66 V for Pt electrode, which



are twice the V_{oc} value of ~ 0.3 V for the samples with only *in-situ* postannealing. If we regard the electrode/LAO/STO system as a metal-insulator-semiconductor structure with zero polar field assumed in the LAO, the observed PV effect could in principle also be explained by an induced potential in the LAO due to the Fermi-level alignment between the STO and the metal electrode. Nevertheless, if this would indeed be the dominant physical origin, the V_{oc} should essentially stay the same for the LAO/STO sample with or without postannealing at atmospheric oxygen pressure, because such postannealing will not alter the band diagram of the LAO/STO system. The observed V_{oc} enhancement upon atmospheric-oxygen-pressure postannealing is largely explained with consideration of the intrinsic polar field in the LAO.

With the thorough cross checks on the various likely complications or artifacts described above, we now can affirmatively attribute the observed PV effects to the intrinsic polar fields surviving in the ultrathin LAO overlayers after charge reconstruction and metal capping. Excitons are photo-excited within the uc-scale LAO films if the photon energy is above the LAO bandgap, and are effectively separated by the strong residual polar fields. The split electrons, in turn, are efficiently collected by the “remotely” placed anode with the assistance of the q2-DEG, while the holes are collected by the surface metal contact.

Discussion

Light-intensity-dependent PV measurements were also performed for the samples with postannealing at atmospheric oxygen pressure, and the results are shown in Fig. 3a. Here the measured V_{oc} exhibits a logarithmic dependence on the incident light intensity. Such a dependence can be understood, because I_{sc} is proportional to the light intensity, while V_{oc} is proportional to $\ln(I_{sc})$, thus the V_{oc} has a logarithmic dependence on the incident light intensity before the internal field is compensated completely by the PV effect³⁵. This behavior has also been observed for PV devices based on coaxial Si nanowires³⁶. Here the V_{oc} is clearly far from its saturated value, even under illumination at the highest available power density of 48 mWcm^{-2} . In this case, the residual polar field has not been compensated completely by the PV effect, and the corresponding band diagrams are depicted in the right panel of Fig. 1a and the Supplementary Fig. S1. The measured V_{oc} should therefore be smaller than V'_{res} .

The PV effect has also been investigated for different LAO thicknesses. For an ideal LAO/STO system with the LAO thickness equal to or larger than the critical thickness of 4 uc, the V_{res} across the LAO is approximately the STO bandgap of 3.2 eV divided by the electron charge, if the LAO/STO band offset is assumed to be zero^{12,20–23}. If the interface is perfect and the light absorption is strong enough, the measured V_{oc} should be V_{res} and V'_{res} without and with the top metal contact taken into account, respectively (see Fig. 1a), and should also be independent on the LAO thickness. However, as shown in Fig. 3b,

the measured V_{oc} for the samples with atmospheric-oxygen-pressure postannealing increases from 0.66 V to 1.03 V as the LAO thickness increases from 5 uc to 15 uc. The observed increase in V_{oc} is reasonable, for example from the consideration that more light is absorbed in the thicker LAO films, thereby driving the PV system closer to the saturation limit.

We can obtain a lower bound estimate on the V_{res} and corresponding residual polar field in the LAO by simply assuming that the V_{res} is equal to the V_{oc} (the actual V_{res} across the LAO should be much larger than the V_{oc} , as discussed earlier). Thus the V_{res} are at least 0.66 V and 1.03 V across the LAO with thickness of 5 uc and 15 uc, respectively, and the corresponding residual polar fields are estimated to be 34 mVÅ^{-1} and 18 mVÅ^{-1} , respectively. These fields are almost 3 orders of magnitude stronger than that in the depletion layer of a typical Si p–n junction²⁸. In the proposed mechanisms to explain the interfacial q2-DEG, a strong polar potential in the LAO even after the emergence of interfacial q2-DEG is a prerequisite for the intrinsic charge reconstruction model^{12,20,21}, while the polar potential should vanish for the structural imperfection mechanisms^{14,17,18}. The observation of a strong residual polar potential as large as 1.03 V favors the charge reconstruction picture. The measured weaker V_{oc} from the V_{res} expected theoretically can be attributed to slight structural disorder, metal contact, and poor light absorption as extensively discussed earlier. In comparison, a residual polar potential of 0.6 V was measured for 5-uc LAO using cross-sectional scanning tunneling microscopy³⁷.

It is worth stressing again that the existence of the residual polar field within the LAO associated with the PV effect indicates that the charge transfer from the LAO surface to the LAO/STO interface is incomplete, namely less than 0.5 electron per 2D uc. As a separate and independent check, we have also directly measured the electron density n_e of the interfacial q2-DEG for different LAO thicknesses, and found that n_e is almost constant (see more details in the Methods), which is consistent with a previous report⁵. This observation differs from the theoretical prediction that n_e increases with LAO thickness^{20,21}, and the discrepancy might be attributed to the localization of some of the transferred electrons^{12,20,21}. In consideration of this observation and the fact that the V_{oc} is smaller than the V_{res} , the possibility of establishing a direct correlation between V_{oc} and n_e is prohibited.

Before closing, we use an illuminating example to briefly highlight the technological relevance of the present study. Fig. 4 demonstrates the normal performance of a commercial CdS photoresistor in response to a green light, driven by a PV device based on the 5-uc-LAO/STO heterostructure. The strong PV effect upon UV radiation also makes LAO/STO a less expensive, scalable, and sensitive alternative material for radiation detection³⁸. Moreover, if the LAO is replaced by another polar material with a smaller bandgap that matches the solar spectrum, a promising solar energy harvester may be expected. This kind of novel PV devices can be seamlessly integrated with the

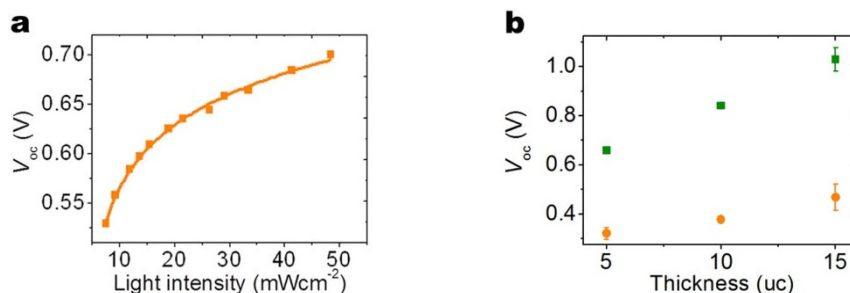


Figure 3 | PV effect dependent on light intensity and LAO thickness. (a) V_{oc} as a function of the light intensity under 6.7-eV light illumination for the atmospheric-oxygen-pressure annealed LAO samples with thickness of 5 uc. Pt electrodes were adopted for the measurements. (b) Measured V_{oc} as a function of the LAO thickness for both the samples with *in-situ* annealing (yellow) and with atmospheric-oxygen-pressure annealing (green), respectively. Au electrodes were adopted for the former, while Pt for the latter.

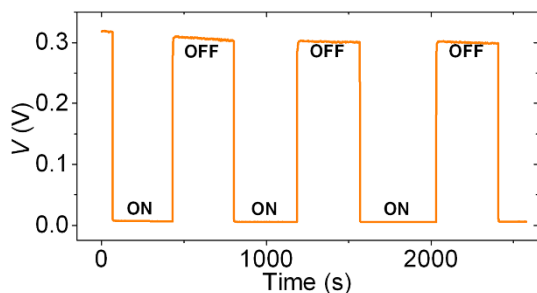


Figure 4 | Power supply to an external resistor. Response of a commercial CdS photoresistor to an on/off-switchable green light source, driven by a prototypical PV device based on a 5-uc-LAO/STO heterostructure.

rapidly developing oxide-based electronic circuitry¹ and even mainstream silicon electronics platforms³⁹. The availability of polar/non-polar oxide heterostructures such as LAO/STO possessing tunable electric polarity and interfacial q2-DEG therefore opens new avenues for realization and integration of PV devices at the fundamental uc-scale limit.

In conclusion, by using PV effect as an effective probe, we have established definitively the existence of a giant residual polar field in the LAO component with a thickness down to a few uc of the polar/nonpolar LAO/STO heterostructures. The lower bound of the measured polar potential across the uc-scale LAO overlayers is 1.0 V. This finding not only provides further insight into the underlying physical origin of the interfacial q2-DEG, but also points to new opportunities in exploring PV materials with atomic-layer control for a wide range of applications.

Methods

Sample preparation. Undoped STO(001) single crystals (CrysTec) were etched using an NH_4F -buffered HF solution after ultrasonic rinsing in deionized water. The crystals were subsequently annealed at 1000°C in an oxygen atmosphere to obtain an atomically flat surface with TiO_2 termination⁴⁰. Next, LAO layers were grown on the treated STO substrates using pulsed laser deposition at 700°C with an oxygen pressure of 1×10^{-4} mbar and a KrF laser. The LAO thickness was monitored *in situ* by reflection high-energy electron diffraction (RHEED) intensity oscillations, as depicted in Fig. 5a. After growth, the samples were annealed at the same growth temperature and oxygen pressure for 1 h and subsequently cooled to room temperature. Some of the samples were further annealed at 600°C for 3 h under atmospheric pressure of oxygen to diminish the oxygen vacancies as far as possible.

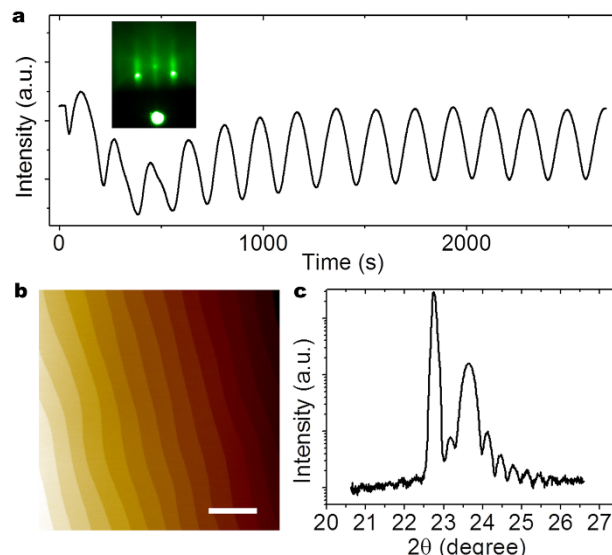


Figure 5 | Sample growth. (a) RHEED oscillations for the LAO overlayer grown on a STO substrate. The inset shows the RHEED pattern after growth of 5-uc LAO layers. (b) AFM image of a 5-uc LAO overlayer on a STO substrate. The scale bar is 1 μm . (c) XRD pattern near the (001) peak of a LAO/STO heterostructure with the LAO thickness of 75 uc.

The large atomic terraces in the atomic force microscopy (AFM) image (Fig. 5b) confirm the flatness of the LAO surface. The superior quality of the LAO/STO heterostructures was further revealed by the fringes near the (001) reflection using X-ray diffraction (XRD) (Fig. 5c); such fringes resulted from the constructive interference of the X-ray beams reflected from the LAO surface and the LAO/STO interface.

Transport measurements. All wires were connected to the LAO/STO interface using ultrasonic welding⁴¹. From our measurements, the LAO/STO interface is insulating for the LAO overlayers thinner than 4 uc, and becomes conducting for the LAO overlayers thicker than 3 uc. The electron density n_e and the mobility μ_e of the interfacial q2-DEG were characterized by measuring the longitudinal resistivity and Hall resistivity at 10 K for the *in-situ* annealed samples. For a 5-uc thick LAO film, the n_e is $3.4 \times 10^{13} \text{ cm}^{-2}$, and the μ_e is $574 \text{ cm}^2\text{V}^{-1}\text{s}^{-1}$. For a 12-uc thick LAO film, the n_e is $3.6 \times 10^{13} \text{ cm}^{-2}$, and the μ_e is $723 \text{ cm}^2\text{V}^{-1}\text{s}^{-1}$. These values are similar to those previously reported⁵.

Vertical transport measurement was performed between an Au (or other metal contact) pad with a thickness of approximately 20 nm sputtered onto the LAO

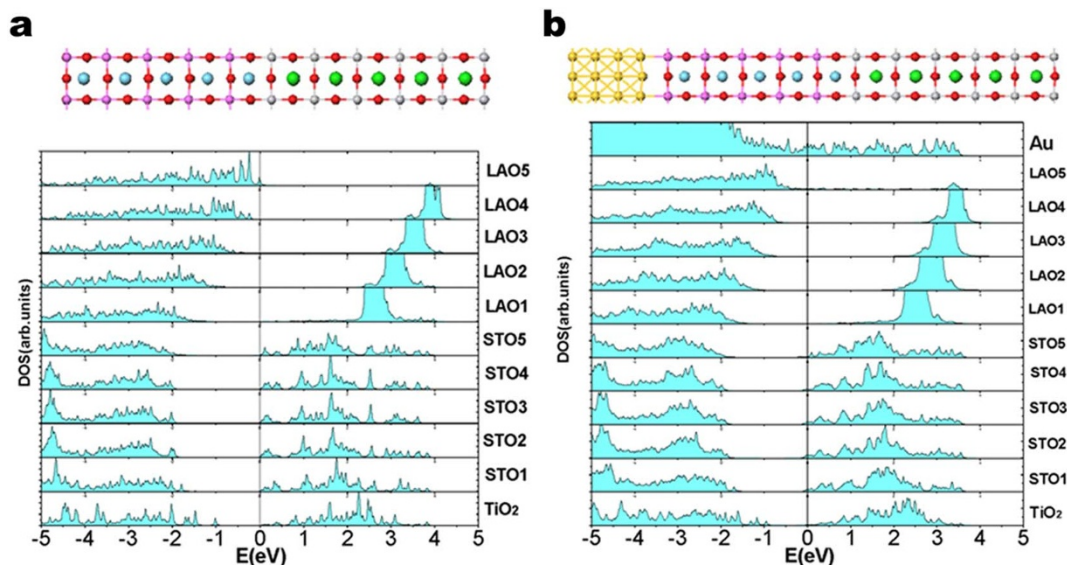


Figure 6 | Theoretical modeling. The optimized atomic structures and corresponding layer-resolved density of states (DOS) of the $(\text{LAO})_5(\text{STO})_{5,5}$ and $\text{Au}_4(\text{LAO})_5(\text{STO})_{5,5}$ slabs, respectively. Zero energy refers to the Fermi level.



surface and an Al wire connected to the LAO/STO interface as depicted in Fig. 1b²⁵. Masks were used to tune the lateral size of the surface electrode. The PV effect was measured between the surface electrode and the Al wire connected to the interfacial q2-DEG as depicted in Fig. 1b under illumination of low-pressure Hg lamps (10 W) with a main peak centered at 6.7 eV and 3.4 eV, respectively. The light intensity was 29 mWcm⁻² unless otherwise specified. We also measured the PV response using a solar simulator (Newport 94023A) with an AM 1.5 G filter (415 W). For the *I*-*V* measurements between the surface electrode and the LAO/STO interface, the latter was set at zero voltage.

We used the PV device based on a 5-uc-LAO/STO heterostructure to drive a commercial CdS photoresistor (Senba Optical & Electronic, model GL55). The LAO/STO heterostructure was under the illumination of a 6.7-eV UV light source, whereas a 2.3-eV green light was adopted to switch on or off the photoresistor.

Theoretical modeling. First-principles density functional calculations were performed using the VASP package^{42–44}. The ion–electron interactions were described by the projector-augmented wave method⁴⁵, and the generalized gradient approximation (GGA) with the spin-polarized PBE functional^{46,47} was used to approximate the exchange–correlation energy of the electrons. A Monkhorst–Pack grid of (7 × 7 × 1) k points was used for the unit cell. (LAO)₅(STO)_{5,5} and Au₄(LAO)₅(STO)_{5,5} slab models as shown in Fig. 6 were adopted in the calculations. An additional TiO₂ layer was adopted to avoid the emergence of a spurious electric field (an approach used in Ref. 27). To test if a 4-layer Au slab can correctly represent the Au electrode, we calculated its work function to be 5.3 eV, in good agreement with the experimental value⁴⁸. The distance between the Au slab and the (LAO)_n slab was approximately 2.7 Å, at which distance good contact between the sample and the electrode is formed. A 12-Å thick area of vacuum was inserted between the neighboring slabs. In order to avoid the interaction between the neighboring slabs, a dipole correction as implemented in VASP was applied. The positions of all the active atoms were allowed to relax until the force on each atom was less than 0.05 eVÅ⁻¹. Finally, we used a 400-eV energy cutoff for geometric optimization and a 500-eV cutoff for the electronic structure.

For an LAO film with thickness of 5 uc, the calculated internal potential and field are 2.2 V and 113 mVÅ⁻¹, respectively without a top Au electrode, which agrees well with previous calculations^{20,21}, and decrease to 1.6 V and 83 mVÅ⁻¹, respectively with the presence of a top Au electrode. The field decreasing after Au capping results from the additional charge transfer from Au to STO near the LAO/STO interface, which further compensates for the polar field in the LAO. We also performed calculations for the LAO/STO with varied LAO thickness larger than 4 uc, and found that the internal potential is basically independent on the LAO thickness, in agreement with previous reports^{12,20,21}.

- Mannhart, J. & Schlom, D. G. Oxide interfaces—an opportunity for electronics. *Science* **327**, 1607–1611 (2010).
- Hwang, H. Y. *et al.* Emergent phenomena at oxide interfaces. *Nat. Mater.* **11**, 103–113 (2012).
- Chakhalian, J., Millis, A. J. & Rondinelli, J. Whither the oxide interface. *Nat. Mater.* **11**, 92–94 (2012).
- Ohtomo, A. & Hwang, H. Y. A high-mobility electron gas at the LaAlO₃/SrTiO₃ heterointerface. *Nature* **427**, 423–426 (2004).
- Thiel, S., Hammerl, G., Schmehl, A., Schneider, C. W. & Mannhart, J. Tunable quasi-two-dimensional electron gas in oxide heterostructures. *Science* **313**, 1942–1945 (2006).
- Brinkman, A. *et al.* Magnetic effects at the interface between non-magnetic oxides. *Nat. Mater.* **6**, 493–496 (2007).
- Reyren, N. *et al.* Superconducting interfaces between insulating oxides. *Science* **317**, 1196–1199 (2007).
- Ariando *et al.* Electronic phase separation at the LaAlO₃/SrTiO₃ interface. *Nat. Comm.* **2**, 188 (2010).
- Dikin, D. A. *et al.* Coexistence of superconductivity and ferromagnetism in two dimensions. *Phys. Rev. Lett.* **107**, 056802 (2011).
- Li, L., Richter, C., Mannhart, J. & Ashoori, R. C. Coexistence of magnetic order and two-dimensional superconductivity at LaAlO₃/SrTiO₃ interfaces. *Nat. Phys.* **7**, 762–766 (2011).
- Bert, J. A. *et al.* Direct imaging of the coexistence of ferromagnetism and superconductivity at the LaAlO₃/SrTiO₃ interface. *Nat. Phys.* **7**, 767–771 (2011).
- Chen, H., Kolpak, A. M. & Ismail-Beigi, S. Electronic and magnetic properties of LaAlO₃/SrTiO₃ interfaces from first principles. *Adv. Mater.* **22**, 2881–2899 (2010).
- Nakagawa, N., Hwang, H. Y. & Muller, D. A. Why some interfaces cannot be sharp. *Nat. Mater.* **5**, 204–209 (2006).
- Cen, C. *et al.* Nanoscale control of an interfacial metal–insulator transition at room temperature. *Nat. Mater.* **7**, 298–302 (2008).
- Siemons, W. *et al.* Origin of charge density at LaAlO₃ on SrTiO₃ heterointerfaces: possibility of intrinsic doping. *Phys. Rev. Lett.* **98**, 196802 (2007).
- Herranz, G. *et al.* High mobility in LaAlO₃/SrTiO₃ heterostructures: origin, dimensionality and perspectives. *Phys. Rev. Lett.* **98**, 216803 (2007).
- Bristowe, N. C., Littlewood, P. B. & Artacho, E. Surface defects and conduction in polar oxide heterostructures. *Phys. Rev. B* **83**, 205405 (2011).

- Qiao, L., Droubay, T. C., Kaspar, T. C., Sushko, P. V. & Chambers, S. A. Cation mixing, band offsets and electric fields at LaAlO₃/SrTiO₃(001) heterojunctions with variable La:Al atom ratio. *Surf. Sci.* **605**, 1381–1387 (2011).
- Willmott, P. R. *et al.* Structural basis for the conducting interface between LaAlO₃ and SrTiO₃. *Phys. Rev. Lett.* **99**, 155502 (2007).
- Son, W.-J., Cho, E., Lee, B., Lee, J. & Han, S. Density and spatial distribution of charge carriers in the intrinsic n-type LaAlO₃/SrTiO₃ interface. *Phys. Rev. B* **79**, 245411 (2009).
- Chen, H., Kolpak, A. M. & Ismail-Beigi, S. First-principles study of electronic reconstructions of LaAlO₃/SrTiO₃ heterointerfaces and their variants. *Phys. Rev. B* **82**, 085430 (2010).
- Cancellieri, C. *et al.* Electrostriction at the LaAlO₃/SrTiO₃ interface. *Phys. Rev. Lett.* **107**, 056102 (2011).
- Cazorla, C. & Stengel, M. First-principles modeling of Pt/LaAlO₃/SrTiO₃ capacitors under an external bias potential. *Phys. Rev. B* **85**, 075426 (2012).
- Segal, Y., Ngai, J. H., Reiner, J. W., Walker, F. J. & Ahn, C. H. X-ray photoemission studies of the metal–insulator transition in LaAlO₃/SrTiO₃ structures grown by molecular beam epitaxy. *Phys. Rev. B* **80**, 241107 (2009).
- Singh-Bhalla, G. *et al.* Built-in and induced polarization across LaAlO₃/SrTiO₃ heterojunctions. *Nat. Phys.* **7**, 80–86 (2011).
- Xie, Y., Bell, C., Yajima, T., Hikita, Y. & Hwang, H. Y. Charge writing at the LaAlO₃/SrTiO₃ surface. *Nano Lett.* **10**, 2588–2591 (2010).
- Arras, R., Ruiz, V. G., Pickett, W. E. & Pentcheva, R. Tuning the two-dimensional electron gas at the LaAlO₃/SrTiO₃ (001) interface by metallic contacts. *Phys. Rev. B* **85**, 125404 (2012).
- Sze, S. M. & Ng, K. K. *Physics of Semiconductor Devices*, 3Edn. (Wiley-Interscience, Hoboken, New Jersey, 2007).
- Peacock, P. W. & Robertson, J. Band offsets and Schottky barrier heights of high dielectric constant oxides. *J. Appl. Phys.* **92**, 4712–4721 (2002).
- Wang, X. *et al.* Ultraviolet photovoltaic effect in tilted orientation LaAlO₃ single crystals. *Physica B* **392**, 104–106 (2007).
- Rastogi, A. & Budhani, R. C. Solar blind photoconductivity in three-terminal devices of LaAlO₃/SrTiO₃ heterostructures. *Opt. Lett.* **37**, 317–319 (2012).
- Tebano, A., Fabbri, E., Pergolesi, D., Balestrino, G. & Traversa, E. Room-temperature giant persistent photoconductivity in SrTiO₃/LaAlO₃ heterostructures. *ACS Nano* **6**, 1278–1283 (2012).
- Guo, E., Lu, H., He, M., Jin, K. & Yang, G. Low-noise solar-blind photodetectors based on LaAlO₃ single crystal with transparent indium-tin-oxide electrode as detection window. *Appl. Opt.* **49**, 5678–5681 (2010).
- Wen, J. *et al.* The substrate thickness dependence of the photovoltage in LaAlO₃-δ/Si heterostructures. *Appl. Phys. Lett.* **94**, 061118 (2009).
- Luque, A. & Hegedus, S. *Handbook of Photovoltaic Science and Engineering*. (Wiley, Chichester, 2003).
- Tian, B. *et al.* Coaxial silicon nanowires as solar cells and nanoelectronic power sources. *Nature* **449**, 885–889 (2007).
- Huang, B. *et al.* Mapping band alignment across complex oxide heterointerfaces. *Phys. Rev. Lett.* **109**, 246807 (2012).
- Pace, E., Di Benedetto, R. & Scuderi, S. Fast stable visible-blind and highly sensitive CVD diamond UV photodetectors for laboratory and space applications. *Diam. Relat. Mater.* **9**, 987–993 (2000).
- Park, J. W. *et al.* Creation of a two-dimensional electron gas at an oxide interface on silicon. *Nat. Comm.* **1**, 94 (2010).
- Koster, G., Kropman, B. L., Rijnders, G. J. H. M., Blank, D. H. A. & Rogalla, H. Quasi-ideal strontium titanate crystal surfaces through formation of strontium hydroxide. *Appl. Phys. Lett.* **73**, 2920–2922 (1998).
- Caviglia, A. D. *et al.* Electric field control of the LaAlO₃/SrTiO₃ interface ground state. *Nature* **456**, 624–627 (2008).
- Kresse, G. & Hafner, J. Ab initio molecular dynamics for liquid metals. *Phys. Rev. B* **47**, 558–561 (1993).
- Kresse, G. & Hafner, J. Ab initio molecular dynamics for open-shell transition metals. *Phys. Rev. B* **48**, 13115–13118 (1993).
- Kresse, G. & Hafner, J. Ab initio molecular-dynamics simulation of the liquid-metal-amorphous-semiconductor transition in germanium. *Phys. Rev. B* **49**, 14251–14269 (1994).
- Kresse, G. & Joubert, J. From ultrasoft pseudopotentials to the projector augmented-wave method. *Phys. Rev. B* **59**, 1758–1775 (1999).
- Perdew, J. P. *et al.* Atoms, molecules, solids, and surfaces: application of the generalized gradient approximation for exchange and correlation. *Phys. Rev. B* **46**, 6671–6687 (1992).
- Perdew, J. P. & Wang, Y. Accurate and simple analytic representation of the electron-gas correlation energy. *Phys. Rev. B* **45**, 13244–13249 (1992).
- Chulkov, E. V., Silkin, V. M. & Echenique, P. M. Image potential states on metal surfaces: binding energies and wave functions. *Surf. Sci.* **437**, 330–352 (1999).

Acknowledgements

This work was supported by the NSFC (91201018, 11034006, 11111140379, 11004179, 11104258, and 21003113), NKBRPC (2009CB929502), “One-hundred-person Project” of CAS, SRFDP (20113402110046), FRFCU (WK2340000011, WK2340000035 and WK2030020017), and CPSFFP (20100470837).



Author contributions

C.Z. conceived the PV experiments and wrote the manuscript. H.L., L.C. and X.Z. prepared and characterized the samples. H.L., L.C., X.Z. and N.P. fabricated the devices and carried out the transport measurements. H.G. and J.Z. performed the theoretical calculations. X.W. and Z.Z. helped on data analysis and presentation. All authors discussed the results and edited the manuscript.

Additional information

Supplementary information accompanies this paper at <http://www.nature.com/scientificreports>

Competing financial interests: The authors declare no competing financial interests.

How to cite this article: Liang, H. *et al.* Giant photovoltaic effects driven by residual polar field within unit-cell-scale LaAlO₃ films on SrTiO₃. *Sci. Rep.* 3, 1975; DOI:10.1038/srep01975 (2013).



This work is licensed under a Creative Commons Attribution-NonCommercial-NoDerivs Works 3.0 Unported license. To view a copy of this license, visit <http://creativecommons.org/licenses/by-nc-nd/3.0>